

# Investigation of dominant degradation mode in field-aged photovoltaic modules using novel differential current-voltage analysis approach

Roopmati Meena  | Manish Kumar  | Rajesh Gupta

Department of Energy Science and Engineering, Indian Institute of Technology Bombay, Mumbai, India

## Correspondence

Roopmati Meena, Department of Energy Science and Engineering, Indian Institute of Technology Bombay, Mumbai, India.  
 Email: [meenaroopmati@iitb.ac.in](mailto:meenaroopmati@iitb.ac.in)

## Abstract

Photovoltaic (PV) modules are susceptible to various types of defects and degradations (D&Ds) under field-operating conditions, which affect their performance and reliability. These D&Ds have non-uniform distribution in the PV modules, which makes it difficult to distinguish amongst multiple D&Ds using a single characterization technique. In the present work, a simple non-destructive characterization approach called differential current-voltage (DIV) analysis using current-voltage (I-V) measurements have been developed for investigation of the dominant degradation mode in the cells of modules, wherein consecutive cells have been partially shaded while measuring the I-V curve of the modules. For this purpose, a batch of crystalline silicon PV modules operating under hot and humid climatic conditions for 20 years has been investigated. A correlation has been established between the trend of percentage change in modules' electrical parameters during DIV measurements and the dominant degradation mode present in the cell under investigation. The trend of change in short circuit current and voltage at maximum power point has been identified as key electrical parameters to identify the dominant degradation mode in the cell. To analyse the trends of DIV analysis, the effect of prominent degradation modes on the module parameters has been investigated using electrical simulations. The investigated PV modules have been cross-characterized through microscopic inspection and electroluminescence imaging to identify various D&Ds present in the investigated modules. The results of cross-characterization substantiate the findings of DIV analysis. The presented DIV approach can be used for the analysis of non-uniform degradation in the PV plants under field-operating conditions.

## KEY WORDS

defects and degradations, differential I-V analysis, EVA discoloration, field-aged PV module, metallization corrosion, non-uniform degradation

**Abbreviations:** c-Si, crystalline-silicon; D&Ds, defects and degradations; DIV, differential current-voltage; EL, electroluminescence; EVA, ethylene vinyl acetate; FF, fill factor; FTIR, Fourier transform infrared thermography;  $I_{mpp}$ , current at maximum power point;  $I_o$ , diode saturation current; IR, infrared;  $I_{sc}$ , short circuit current; I-V, current-voltage; LED, light emitting diode; LIT, lock-in thermography; MPP, maximum power point; n, diode ideality factor; O&M, operations and maintenance; PV, photovoltaic; QE, quantum efficiency;  $R_s$ , series resistance;  $R_{sh}$ , shunt resistance; SD, standard deviation; SDM, single diode model; SEM, scanning electron microscopy; UAV, unmanned aerial vehicles; UVF, ultraviolet fluorescence;  $V_{mpp}$ , voltage at maximum power point;  $V_{oc}$ , open circuit voltage; XRD, X-ray diffraction;  $\mu$ , mean.

## 1 | INTRODUCTION

Silicon-based photovoltaic (PV) modules are commercially most successful PV technology comprising over 95% of the module production worldwide and find application in multiple forms, namely, large grid-connected PV fields, hybrid wind-solar farms, and stand-alone microgrids.<sup>1–3</sup> Owing to large-scale installations, c-Si PV modules must provide reliable output power for the stipulated warranty period to ensure a timely return on investment. However, the c-Si PV module is a multi-layered structure susceptible to various types of defects and degradations (D&Ds), that is, structural, chemical and optical.<sup>4,5</sup> These D&Ds can originate at different stages of a PV module lifespan from manufacturing, transportation and installation to field-operation. Under field-operating conditions, PV modules are subjected to various types of environmental stresses like high temperature, cyclic temperature variation due to day and night, high humidity, ultraviolet (UV) radiation, high wind speed and hailstorm.<sup>6,7</sup> These stresses tend to induce D&Ds in one or more components of module which eventually reduces the module reliability impacting its output power. Some of the prominent D&Ds which impact the output power of modules under field-operating conditions are encapsulant degradation, finger and busbar corrosion, snail-trails, interconnect ribbon degradation, micro-cracks and their progression into cracks, soiling and backsheet delamination.<sup>8–11</sup> The prominent D&Ds can be broadly classified into two categories based on their effect on the output electrical parameter as encapsulant degradation (discoloration and delamination) and metallization degradation (metallization corrosion, interconnect ribbon burnout, finger interruptions, etc.).<sup>12–14</sup> These D&Ds usually have a non-uniform distribution in the field-aged PV modules.

Multiple studies have performed investigations on field-aged PV modules to understand various degradation modes.<sup>15–18</sup> Yedidi et al.<sup>19</sup> have investigated 16-year-old PV modules using current-voltage (I-V) curve measurements and infrared (IR) thermography. An average degradation rate of 1.1%/year has been calculated primarily due to encapsulant degradation and thermo-mechanical fatigue related failure. Similarly, Polverini et al.<sup>20</sup> has done comparative analysis of pre- and post-installation I-V data on 20-year-old polycrystalline PV modules installed in a subtropical climate. Severe discoloration and metallization corrosion were found to be the primary cause of overall performance decay of 4.42%. Chandel et al.<sup>21</sup> have performed degradation analysis on 28-year-old PV modules integrated with a water pumping system installed in the Himalayan region. They have reported a degradation rate of 1.4% in the investigated modules. It has been attributed to loss in short circuit current ( $I_{sc}$ ) and fill factor (FF) owing to severe discoloration and delamination of encapsulant, oxidation of metal fingers and bubbling in the backsheet. In addition to analysing the rate of degradation in PV modules, in-depth analysis on field-aged modules has also been performed using multiple characterization techniques in tandem.<sup>22–24</sup> For example, Buerhop et al.<sup>25</sup> have investigated about 260 dismantled modules using electroluminescence (EL) imaging, I-V curve measurement and IR thermography to study the impact of cell cracks, solder joint failure and short-

circuited cells on the resulting module temperature and the power output. Meena et al.<sup>26</sup> have performed comparative analysis between encapsulant discoloration and delamination using Fourier transform infrared (FTIR) spectroscopy, quantum efficiency (QE) and X-ray diffraction (XRD), wherein they have reported absorption and reflection of incident irradiance from the discoloured and delaminated encapsulant surfaces, respectively, as the main loss incurring mechanism. For in-depth analysis of various D&Ds, PV modules have to be unmounted from the field and analysed in controlled lab conditions using sophisticated characterization techniques. However, early diagnosis of non-uniform degradation in field conditions is also necessary for improvement of overall PV system operations and maintenance (O&M).

Some of the characterization techniques used for in-field investigation of PV modules are I-V curve measurement, EL imaging and IR thermography.<sup>27,28</sup> The imaging characterization techniques have also been integrated with drone-based systems for in-field inspection of large PV plants.<sup>29,30</sup> Francesco et al.<sup>31</sup> have used drones equipped with visual and IR sensors to monitor and investigate multiple ground and rooftop mounted PV plants under operating conditions in Italy. They have correlated different types of D&Ds observed from visual images with the high temperature regions in the IR images. Benatto et al.<sup>32</sup> and Koch et al.<sup>33</sup> have investigated the viability of EL imaging for large scale PV plant inspection. They have highlighted the limitation of EL imaging under the influence of irradiance, wind and daylight, wherein noise characteristics dominate due to interference in the EL signal from daylight. In addition to EL imaging and IR thermography, I-V curve measurement is the most commonly used in-field characterization technique. For this purpose, the I-V curve tracers installed with the PV module arrays are utilised for primary analysis of D&Ds. Sastry et al.<sup>34</sup> have investigated mono c-Si PV modules from 11 different module manufacturers exposed to identical field conditions for 10 years using I-V data. The electrical performance parameters have been analysed as a function of time of field exposure. The overall degradation found in the modules has been higher than expected for the investigated timeframe.

Conventional methods of I-V curve analysis provide information pertaining to reduction in module's overall performance.<sup>35,36</sup> However, it fails to highlight the non-uniform distribution of D&Ds in PV modules. In this regard, Sinha et al.<sup>15</sup> have applied partial shading over the cells of crystalline silicon PV modules to investigate uneven discoloration in crystalline silicon PV modules. In another study, Alers et al.<sup>37</sup> have simulated the effect of partial shading over the cells of a PV module to calculate the value of shunt resistance in respective cells. However, in both the previous studies, characteristics pertaining to a single degradation mode has been examined. In the present study, the application of partial shading has been extended to examine the dominant degradation modes in the cells of a PV module suffering from multiple types of D&Ds simultaneously. Herein, a novel approach using differential I-V (DIV) measurement has been developed to identify the dominant D&Ds in the cells of a module. The proposed approach examines the current and voltage distribution in a string of cells when one of the cells becomes

current-limiting. In the presented approach, each cell has been made current limiting by sequentially shading the cells in a module and trend of change in electrical parameters of the module has been analysed. The trends have been correlated with the dominant degradation in the cells such as encapsulant and metallization degradation. In order to corroborate the results of the DIV approach, the dominant D&Ds have also been identified by cross-characterization of the investigated modules using EL imaging and microscopic inspection. Further, simulation has been performed to understand the effect of individual D&Ds on electrical parameters of the module to support the results of DIV analysis.

The outline of this paper is as follows. Section 2 describes the methodology adopted and details of the techniques used in this work. Section 3 contains the results pertaining to dominant D&Ds in the cells of the modules and their identification using the DIV approach. The findings of this work have been concluded in Section 4.

## 2 | METHODOLOGY

In this work, field-aged PV modules having non-uniform degradation have been systematically analysed for the identification of dominant modes of degradation in their cells using a novel approach of DIV measurements. The flowchart showing the schematic of the

methodology used in this study is given in Figure 1. A batch of 20 field-aged modules installed for 20 years under hot and humid climatic conditions of Mumbai, India, has been investigated and subjected to DIV analysis. The specifications of the modules are given in Table 1. These modules have been cross-characterized through microscopic inspection and EL imaging technique. The results of DIV analysis have been substantiated with the findings of the cross-characterization to identify the degradation modes in modules.

The microscopic inspection has been performed using a 1600 × 1200 pixel digital microscope. It has a dual magnification 400X lens with 8X white light LEDs. The preliminary analysis was performed using visual inspection and I-V curve measurements to identify the severity of D&Ds in batches of field-aged modules. The results of four module are presented here, which represent and summarize the D&Ds observed in the batch of investigated PV modules. They have been named FA-01, FA-02, FA-03 and FA-04 henceforth. These modules have been cross-characterized using EL imaging and microscopic inspection. Concurrently, the modules have been subjected to non-destructive analysis using DIV measurements to identify the dominant degradation modes in its solar cells. These dominant degradation modes have been correlated with the trend of percentage change in electrical parameters of the modules during DIV measurements. Also, the change in electrical parameters due to distinct degradation modes has been studied separately using electrical simulations.

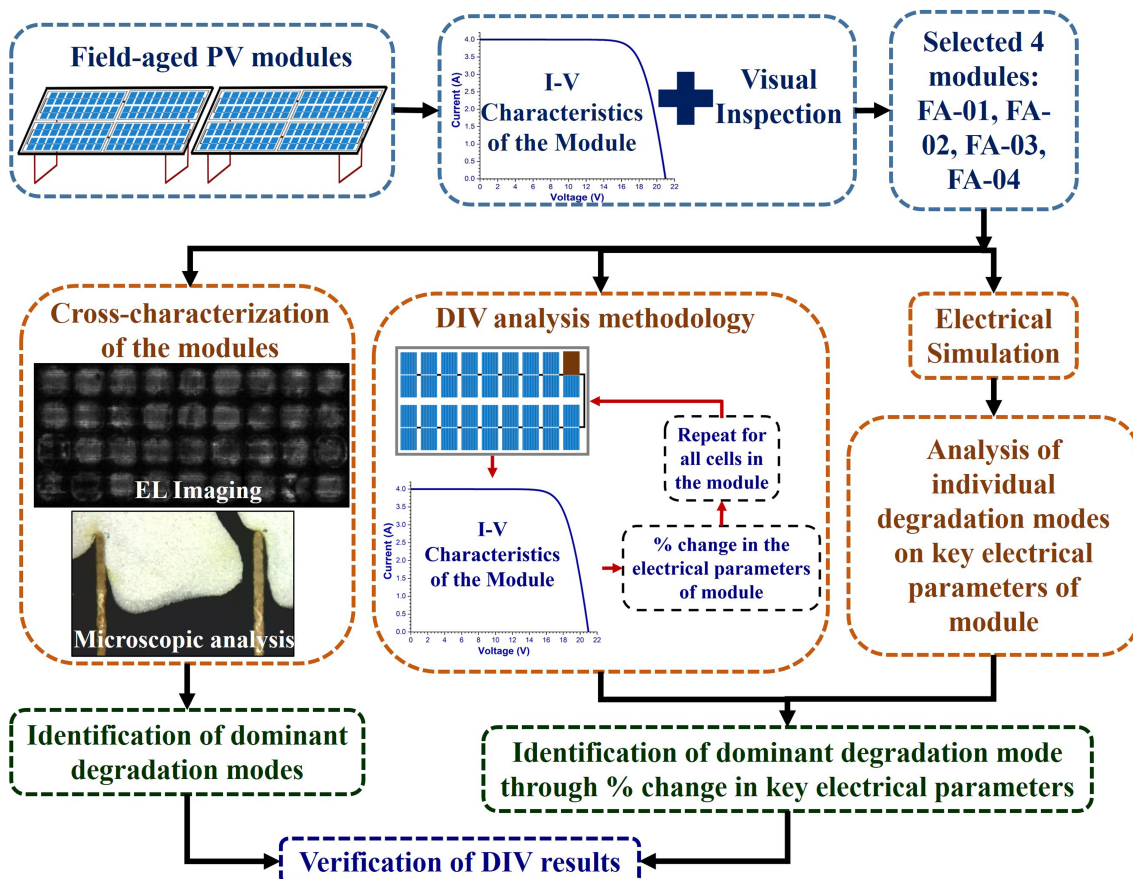


**FIGURE 1** Schematic of the methodology used in this study

**TABLE 1** Specifications of the field-aged PV modules

Parameters	Values
No. of cells in the module	36
Cell area	$15.6 \times 15.6 \text{ cm}^2$
Type of solar cell	Mono-crystalline
Open circuit voltage	22 V
Short circuit current	4 A
Maximum output power	60 W

Finally, the results obtained from DIV analysis and the observation from the cross-characterization of the modules have been correlated to validate the DIV analysis results. The detailed approach followed for DIV analysis of the module has been described in the next subsection.

## 2.1 | DIV analysis approach

A non-destructive approach using DIV measurement has been developed to investigate the dominant mode of degradation in the solar cells of the PV modules subjected to non-uniform degradation under external operating conditions. In this approach, each cell of the module has been partially shaded while measuring the module's I-V curve. During partial shading, the output parameters of the module depend on characteristics of the weakest, current-limiting cell in the module. In DIV analysis approach, each cell of the module has been sequentially made the current-limiting cell by applying partial shading over it. However, the extent of partial shading has been applied considering non-uniform distribution of defects and degradations in cells of the modules. The shading pattern has to be higher than the other current effecting D&Ds in the cell to make it the current-limiting cell of the module during DIV analysis. For this purpose, the shading area of 50% has been found to be optimum as it was higher than the extent of discoloration over the cells. However, the extent and type of partial shading applied on all the cells have been the same. Thus, the variation in the change of electrical parameters of the module with partial shading of the consecutive cells can be attributed to the pre-existing D&Ds modes in the cell under investigation. The percentage change in the electrical parameters of the module has been evaluated relative to unshaded module parameters. In this regard, the percentage change in  $I_{sc}$ , voltage at maximum power point ( $V_{mpp}$ ) and current at maximum power point ( $I_{mpp}$ ) have been analysed in detail to determine the underlying dominant degradation mode in the shaded cell. It must be noted that each investigated module had 36 series-connected cells and two bypass diodes, each connected across the string of 18 cells. The string with 18 cells and one bypass diode is called a submodule henceforth. The comparative analysis between change in electrical parameters of submodules during DIV has also been performed. The electrical parameters of the modules have been calculated from the illuminated I-V curve measurement. The I-V measurements have been performed at standard test conditions (AM1.5G,

25°C and 1000 W/m<sup>2</sup>) using a module simulator (QuickSun-700). Further, spatial characterization has been performed using EL imaging and visual inspection to substantiate the result obtained from DIV measurements.

## 2.2 | EL imaging

EL imaging has been performed on the selected field-aged PV modules after I-V curve measurement and visual inspection. The EL imaging technique works on the principle of emission of IR radiation from the solar cell during the electrical biasing of the module. The IR radiation emission from solar cells has been captured using Greateyes (GE BI MID) EL camera with a 1024 × 1024-pixel silicon-charged coupled device (Si-CCD) detector and processed in the dedicated software on a computer. The modules have been imaged from the front-glass side. For this purpose, they have been biased at  $I_{sc}$  using a programmable power supply while capturing the images. The experiment to capture EL image has been performed under a dark enclosure at 25°C to avoid interference from stray lights. The EL imaging technique has been coupled with microscopic inspection for cross-characterization of various D&Ds in the investigated modules.

## 2.3 | Electrical simulation

The electrical simulations have been performed to understand the independent effect of non-uniform distribution of different degradation modes on the electrical parameters of the module. Figure 2 provides the schematic of the PV module used for the simulation study. It consists of 36 series-connected cells divided into two submodules, each consisting of 18 cells and a bypass diode. The solar cells have been modelled using the single diode model (SDM).<sup>38</sup> The SDM has been defined using five parameters and consists of a current source ( $I_{sc}$ ), a diode, series resistance ( $R_s$ ) and shunt resistance ( $R_{sh}$ ). The five parameters for SDM, namely,  $I_{sc}$ , diode saturation current ( $I_o$ ), diode ideality factor ( $n$ ),  $R_s$  and  $R_{sh}$  have been extracted from the module datasheet using analytical equations given by Kumar et al.<sup>39</sup> The value of parameters used to define SDM is given in Table 2. The simulations have been performed in PSpice circuit simulator software. Different degradation modes have been modelled by varying one of the five parameters in the SDM of the solar cell. The effect of different degradation modes has been analysed on the electrical parameters of the module, namely,  $I_{sc}$ ,  $I_{mpp}$ ,  $V_{mpp}$  and maximum power point (MPP).

## 3 | RESULTS AND DISCUSSION

### 3.1 | Investigation of degradation modes in PV modules

This section presents the results of module investigation through various spatial and non-spatial characterization techniques. The selected

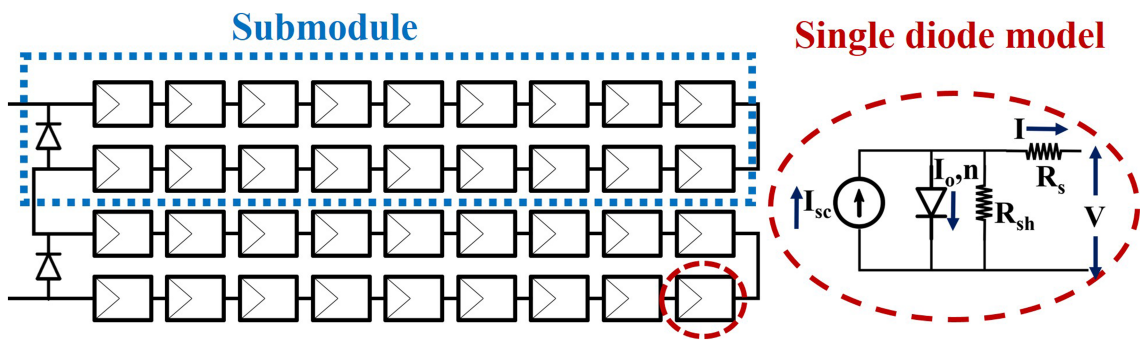


**FIGURE 2** Schematic of the PV module used for electrical simulation

**TABLE 2** Values of parameters for SDM used in this study

Parameter	$I_{sc}$	$I_o$	$n$	$R_s$	$R_{sh}$
Value	4 A	$1.56 \times 10^{-6}$ A	1.55	0.009 $\Omega$	8.92 $\Omega$

modules have been thoroughly investigated for various types of D&Ds through visual and microscopic inspection, I-V curve measurement and EL imaging technique.

### 3.1.1 | Visual and microscopic inspection

The field-aged PV modules have been investigated for prominent types of D&Ds through visual and microscopic inspection. Figure 3 shows the various types of D&Ds found in the majority of the investigated modules. These D&Ds had non-uniform distribution over the cells in the modules. In this regard, non-uniform discolouration in the ethylene vinyl acetate (EVA)-based encapsulant over the solar cells has been observed as shown in Figure 3A. It can be observed that within a cell, region-A is transparent compared to region-B, which has a brown appearance. Moreover, the periphery area of the cell is also similar to region A in appearance. Based on the available literature, discoloured EVA is reported to become transparent due to the photo-bleaching phenomenon in the presence of moisture and air.<sup>40</sup> In addition to discolouration, delamination between encapsulant and solar cell has also been observed in the modules. In most of the cells, the delamination was confined in a small region along the busbar length. However, for the cells over the junction box, it was present in the extended area as shown in Figure 3C. The large delaminated region over the junction box region coincides with the prevalence of high temperature and moisture conditions, reported to be responsible for initiation and progression of delamination in the modules.<sup>24</sup> Based on the above analysis, it can be said that encapsulant degradation has been one of the prominent degradation modes in the investigated modules.

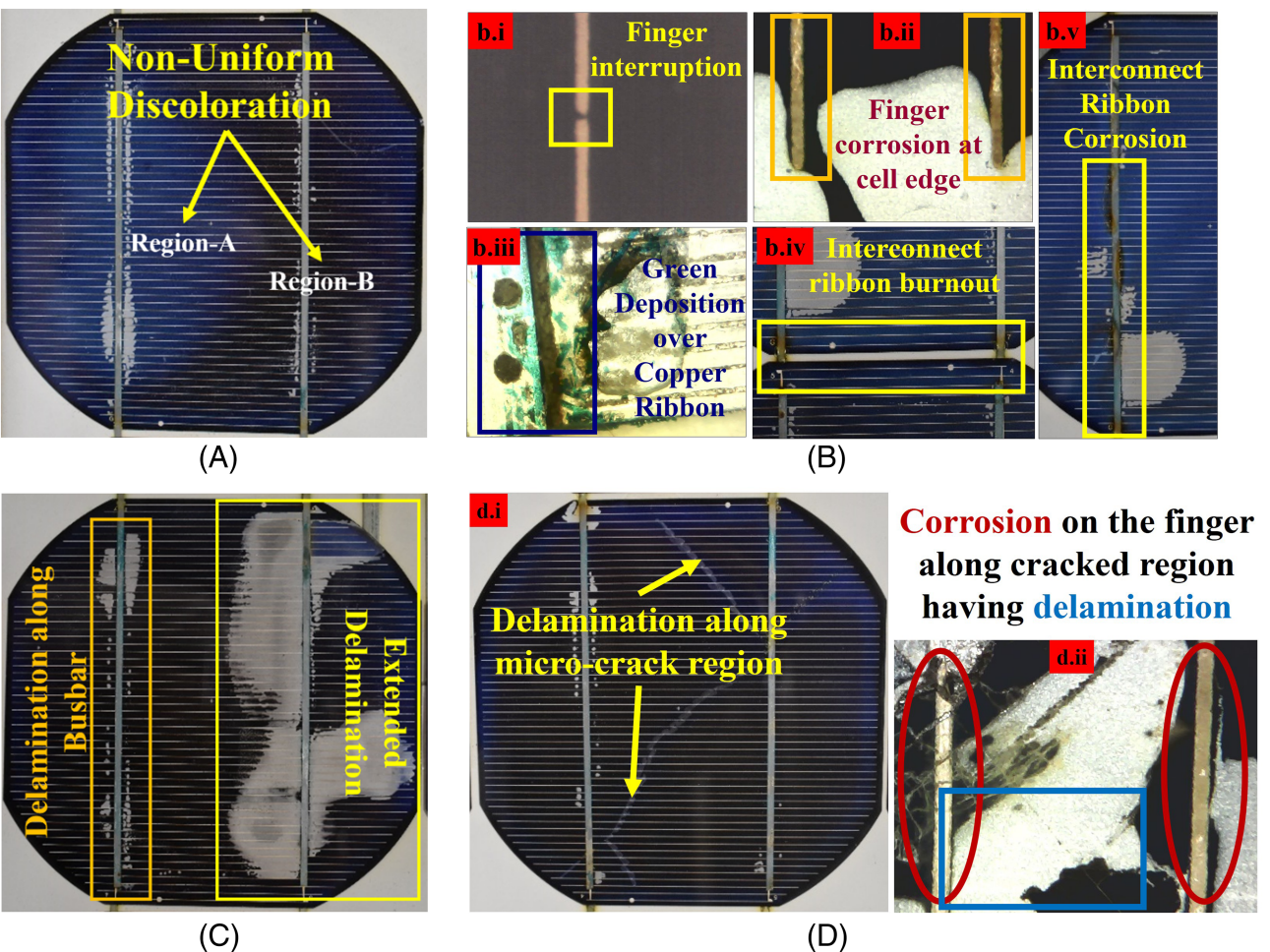
In addition to EVA degradation, degradation in cell metallization and interconnect ribbon have also been observed during the microscopic inspection of the modules. Different types of metallization D&Ds found are shown in Figure 3B. Finger interruption as shown in

Figure 3B.i has been observed in multiple cells. Also, fingers along the edges of the solar cell and at the delaminated regions had brown-coloured deposition over them as shown in Figure 3B.ii. The interconnect ribbon also had green and brown coloured deposition over them as shown in Figure 3B.iii,b,v, respectively. The observed depositions over fingers and interconnect ribbon occur due to corrosion of constituting metal components, that is, silver paste and copper, respectively. The corrosion is facilitated by the moisture and air ingestion along the cell edges through white space between cells, along delaminated busbar regions, through micro-cracks in the cell, and so forth. Moreover, cell metallization has also been reported to be corroded by the acetic acid released during EVA discoloration.<sup>41</sup> The interconnect ribbon at the edge of adjoining cells had burnout marks as shown in Figure 3B.iv. In addition to encapsulant and metallization degradation, some modules also had micro-cracks, which were visible due to delamination along their length as shown in Figure 3D.i. The micro-cracks can originate at various stages of PV module lifespan ranging from manufacturing, transportation, installation and operation in the field.<sup>42</sup> These micro-cracks provide a preferential path for moisture and air ingressions, which can lead to corrosion of cell metallization and interconnect ribbon lying along its length as shown in Figure 3D.ii.

The analysis performed using visual and microscopic inspection provides primary information about the D&Ds in the modules; however, the extent and severity of D&Ds cannot be quantified. Thus, I-V curve analysis has been performed on the investigated modules as discussed in the subsequent section.

### 3.1.2 | Current–voltage (I–V) curve measurement

The various D&Ds observed during visual and microscopic inspection result in the loss of electrical parameters of the module. The cumulative loss incurred in the electrical parameters of the modules has been quantified through I-V curve measurements. In this regard, the change in electrical parameters of modules, namely,  $I_{sc}$ , open circuit voltage ( $V_{oc}$ ), MPP and FF, have been calculated with respect to the rated parameters. The bar graph showing the percentage change in the electrical parameters is given in Figure 4. A significant degradation in  $I_{sc}$  and MPP can be observed for all investigated modules, wherein maximum degradation has been observed for the module FA-02 of up to



**FIGURE 3** (A) Non-uniform discoloration, (B) cell metallization and interconnect ribbon degradation, (C) delamination and (D) micro-crack and corrosion along its length

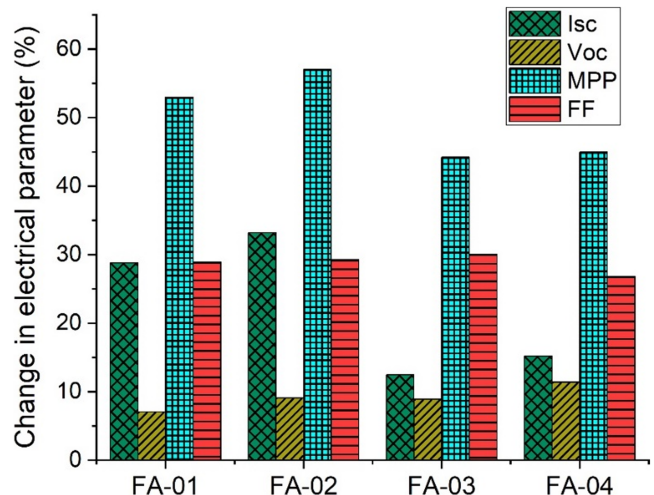


**FIGURE 4** Percentage change in the electrical parameters of the investigated PV modules

33% and 57% in I<sub>sc</sub> and MPP, respectively. The loss in I<sub>sc</sub> can primarily be attributed to the EVA discoloration in the modules. The discoloured EVA blocks the incident irradiation from reaching the solar

cell, thus reducing light-generated current, I<sub>sc</sub>. The loss in MPP can be attributed to the cumulative effect of multiple types of D&Ds which affect the operation of the modules. The effect of these D&Ds can also be observed as the loss in FF of the modules. The FF in a module gets affected by an increase in R<sub>s</sub> caused by the corrosion of fingers, busbar and interconnect ribbon, micro-cracks, finger interruption, and so forth. A maximum degradation of up to 30% has been calculated in FF. The I-V curve analysis is useful in quantifying the overall degradations in the module. However, it does not provide spatial insights on the types and nature of D&Ds, which is crucial to determine the severity and location of the defects in the degraded modules. Thus, for spatial analysis of D&Ds, EL imaging has been performed as discussed in the next section.

### 3.1.3 | EL imaging

EL imaging technique has been used to analyse the spatial distribution of D&Ds in the field-aged modules. The dark region in the EL image corresponds with the presence of D&Ds in the module. Based on the pattern of the dark regions in EL image, different types of degradation

modes in the modules can be identified. The EL images of the investigated modules are given in Figure 5. The module FA-01, as shown in Figure 5A, has dark circular patterns over the majority of its solar cells (encircled in red). It corresponds to the presence of encapsulant discoloration, which blocks the IR radiation emitted from the cells during EL measurements. However, the periphery region along the edges of the cell is bright due to the photo-bleaching of the discoloured EVA. Non-uniform photo-bleaching has resulted in non-uniform discoloration over the cells, as observed in the visual inspection of the PV modules (Figure 3A). The regions corresponding to non-uniform discoloration have irregular dark patterns over the cells in the EL images (encircled in green) as visible in the Figure 3B-D of modules FA-02, FA-03 and FA-04, respectively. It must be noted that irregular dark patterns in EL images have also been reported for recombination sites in cells. It makes it difficult to distinguish the recombination sites from non-uniform discoloration. In addition to dark patterns corresponding to discoloration, the EL image of FA-03 has another type of dark pattern in a few of its cells (encircled in blue). The region around the busbar has a dark appearance in the EL images, but the region between the busbar appears bright. However, during visual and microscopic inspection, the region corresponding to the aforementioned dark patterns in FA-03 has not shown any sign of degradation. Such dark patterns around the busbar in EL images without visible degradation have been reported to occur due to solder material degradation from underneath interconnect ribbon-busbar assembly.<sup>43</sup>

The presence of discoloration over the majority of the solar cells has hindered the detection of other types of prominent degradation modes through EL imaging, which were observed during the visual and microscopic inspection. Herein, the corrosion on the fingers along the micro-cracks and delaminated region in FA-01 cannot be observed in its EL image (Figure 5A). However, in some modules, the region along the cell edges had an extended dark appearance (encircled in

yellow) corresponding to the finger corrosion observed in the microscopic inspection. Corrosion of the fingers and busbars obstructs the flow of current to the silicon wafer. As a result, EL signals do not originate from the cell region which has corroded metallization causing dark appearance. Moreover, the region corresponding to the micro-crack in FA-02 is visible as a sharp pattern (encircled in purple) in Figure 5B. However, micro-cracks present in other modules are not visible in the corresponding EL images because of the severe discoloration on the solar cells. Though the EL imaging technique has been widely adopted for inspection of modules, it must be noted that different modes of D&Ds are difficult to distinguish in the EL images of modules having non-uniform degradation. In addition, some degradation modes physically present in the modules cannot be detected in the EL image due to the superposition by other severe degradation modes. Therefore, the DIV analysis has been explored in this work to qualitatively examine the prominent modes of degradation in the cells of modules using I-V curve measurement.

### 3.2 | DIV method

The commonly available analysis methods used to examine the modules, namely, I-V curve measurement and EL imaging technique, are unable to distinguish amongst various non-uniform D&Ds mechanisms operational in the cell of the modules. The I-V curve measurements only provide information regarding the overall degradation in the module. Similarly, EL images alone cannot distinguish between distinct D&Ds as they can all appear as dark regions. This makes it difficult to identify the extent of non-uniform degradation in the modules. In this regard, to identify and investigate non-uniform degradation in the modules, DIV analysis approach has been developed in this work, wherein a correlation has been established

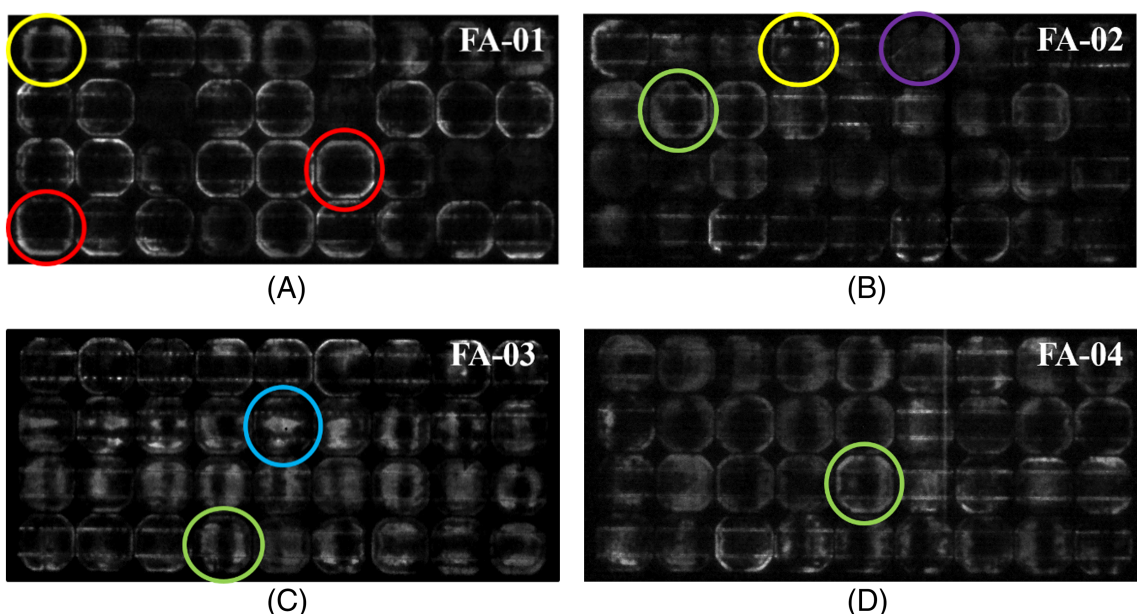


**FIGURE 5** Electroluminescence images of the module (A) FA-01, (B) FA-02, (C) FA-03 and (D) FA-04

between the trend of change in electrical parameters of the module and prominent degradation modes present in the cells of the module.

### 3.2.1 | Analysis of measured electrical parameters

The percentage change in the electrical parameters of the module has been calculated with respect to electrical parameters measured without partial shading of cells for DIV analysis. Herein, the trend of the percentage changes in electrical parameters has been correlated with the prominent degradation modes observed in the solar cells through cross-characterization. In this regard, the percentage change in  $I_{sc}$ ,  $I_{mpp}$ ,  $V_{mpp}$  and MPP has been studied in detail.

The percentage change in  $I_{sc}$  and  $V_{mpp}$  corresponding to the sequential partial shading of solar cells for all the investigated modules is given in Figure 6. It can be observed that the percentage change in  $I_{sc}$  has been found positive implying decrement in the  $I_{sc}$  value during DIV measurements. The loss in  $I_{sc}$  can be attributed to the cumulative effect of applied partial shading and pre-existing D&Ds in the investigated solar cells. However, the extent of shading applied over all the cells during DIV measurements has been the same. Thus, the variation in the percentage change for different cells of the modules can be attributed to the degradation modes already present in the solar cells. In this regard, the cells in the two submodules of a module have been comparatively analysed for non-uniformity in the degradation modes. It can be observed from Figure 6A.i,c,i,d.i that for modules FA-01, FA-03 and FA-04, cells in one of their submodules have a higher change in  $I_{sc}$  compared to another. While for the module FA-02 shown in Figure 6B.i, the variation in  $I_{sc}$  during DIV measurements has been less between two submodules.

One of the major degradation modes which effects the  $I_{sc}$  of a cell is encapsulant discoloration. It hinders the transmission of incoming radiation thus reducing the  $I_{sc}$  of the solar cell. Discoloration has been observed in all the investigated modules. However, the modules had the non-uniform distribution of discoloration on the cells within a module. Thus, the effect of discoloration on  $I_{sc}$  would vary within cells of the module. The most discoloured cell in the series-connected cells of a submodule would have the lowest  $I_{sc}$ , thus would become the current limiting cell of the submodule. However, during DIV measurements, each cell under investigation has intentionally been made the current limiting cell of the submodule by applying partial shading over it. The effect of shading over a cell would vary based on the extent of discoloration. The cell with a higher extent of discoloration would have less reduction in  $I_{sc}$  during DIV measurements, while a cell with a lower extent of discoloration would have a higher reduction in  $I_{sc}$ . Thereby, the submodule with less discoloured cells would result in comparatively higher  $I_{sc}$  change with respect to another submodule. Thus, the difference in the extent of  $I_{sc}$  change within the submodules of FA-01, FA-03 and FA-04 could be attributed to the non-uniform discoloration on cells in their respective two submodules. Furthermore, variation within a submodule indicates non-uniform discoloration within the cells of the submodule.

The presence of non-uniform D&Ds in the cells of the module would also change the operating point of the module during DIV measurements. The change in the value of current at the operating point, that is,  $I_{mpp}$  during DIV measurement, would take into account the cumulative effect of major pre-existing D&Ds and shading in the cell. While the extent of partial shading applied has been similar, the change in electrical parameters at the operating point, that is,  $I_{mpp}$  and  $V_{mpp}$  of the module, would depend on the major pre-existing D&Ds in the cell under investigation. It was observed that the trend of

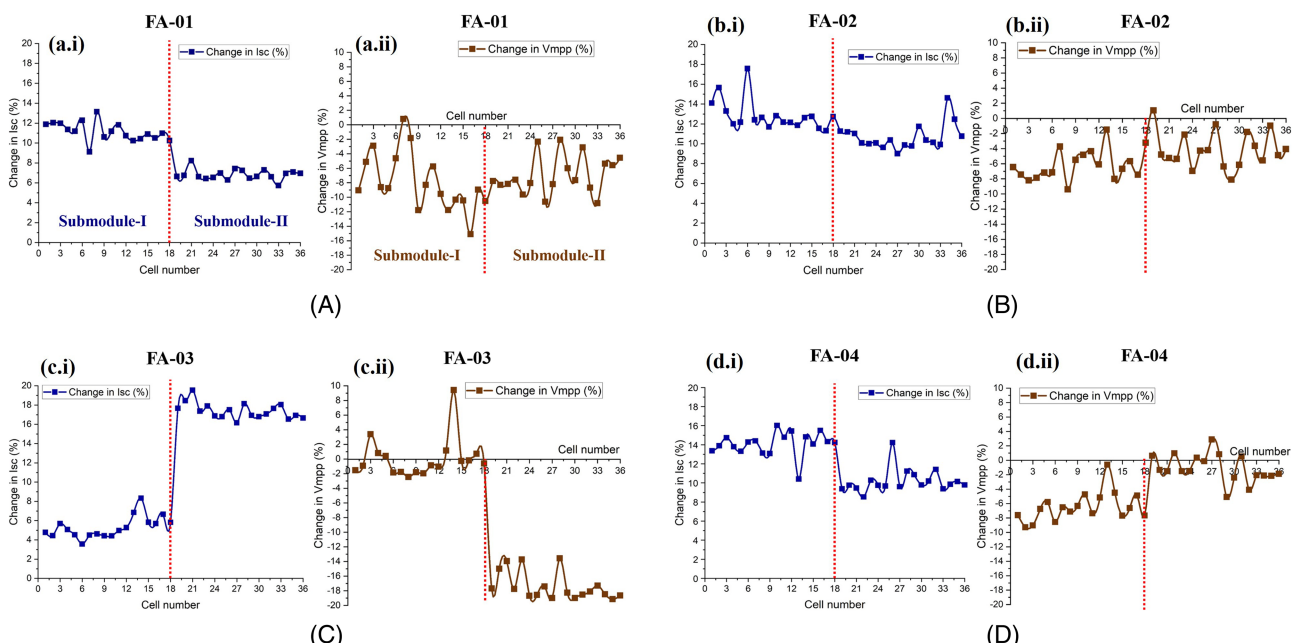


**FIGURE 6** Percentage change in  $I_{sc}$  and  $V_{mpp}$  during DIV measurements for module (A) FA-01, (B) FA-02, (C) FA-03 and (D) FA-04

percentage change in  $I_{mpp}$  has been similar to that in  $I_{sc}$ . Thus, in order to avoid repetition of graphs, the graphs showing percentage change in  $I_{sc}$  have been used to explain the results pertaining to trend of change in  $I_{mpp}$ .

The change in  $I_{mpp}$  of a submodule during DIV measurements would cause the unshaded cells to operate at low efficiency. It causes the value of operating voltage, that is,  $V_{mpp}$  of unshaded cells to move towards their  $V_{oc}$ . Since the resultant voltage across a submodule is the cumulative sum of the voltages across its individual cells, the module  $V_{mpp}$  increases due to a decrease in the  $I_{mpp}$  in a submodule. It implies that higher positive percentage change in current (i.e., loss in  $I_{mpp}$ ) would cause a high negative change in  $V_{mpp}$  and vice-versa. This trend has been observed for the percentage change in  $V_{mpp}$  of the modules FA-03 and FA-04 as shown in Figure 6C.ii,d.ii, respectively, wherein, for the module FA-03, the submodule-I has a comparatively less negative change in  $V_{mpp}$  than its submodule-II, thus agreeing with the trend observed in the percentage change in  $I_{sc}$ , as shown in Figure 6C.i. Similarly, for module FA-04, the change in  $V_{mpp}$  is more negative in submodule-I than its submodule-II which has comparatively lower  $I_{sc}$  change in its cells (Figure 6D.i). However, for FA-01 and FA-02, the change in  $V_{mpp}$  does not have distinction along the submodules nor any direct correlation could be established with the trend of change in  $I_{sc}$ . It could be due to the effect of other types of D&Ds in its cells. It must be recalled that in addition to encapsulant discoloration, the second major type of D&Ds observed in the investigated modules has been the corrosion of finger, busbar and interconnect ribbon, micro-cracks, finger interruption and interconnect burnouts. These D&Ds directly affect the  $R_s$  of the cell. Thus, in order to understand the effect of the non-uniform distribution of  $R_s$  and  $I_{sc}$  on the module parameters, electrical simulations have been performed as discussed in the next subsection.

### 3.2.2 | Analysis of electrical parameters using simulation

Electrical simulation has been performed to understand the effect of non-uniform degradation on the electrical parameters of the module. Herein, the prominent degradation modes identified through visual inspection and I-V curve measurements have been modelled in the simulation. Degradation in encapsulant and metallization corrosion had been identified as the two prominent degradation modes. These dominant degradation modes have been modelled by varying the one of the five parameters in the SDM of the solar cell in accordance to their loss incurring mechanism. In this regard, the encapsulant degradation has been modelled as change in  $I_{sc}$ , while the metallization degradation has been modelled as a change in  $R_s$  in the SDM. However, as observed during primary analysis of the modules, various D&Ds had non-uniform distribution in the investigated modules. Thus, to understand the independent effect of the non-uniform distribution of encapsulant and metallization degradation, the concerned parameter in SDM has been varied, and its effect on the modules electrical parameters ( $V_{mpp}$ ,  $I_{mpp}$  and MPP) has been analysed. In order to model

the non-uniform degradation in the simulation, randomization has been used, wherein each solar cell in the module has been assigned a unique value of  $I_{sc}$  and  $R_s$ , respectively. These unique values of  $I_{sc}$  and  $R_s$  for each cell have been generated using the mean ( $\mu$ ) and standard deviation (SD) of  $I_{sc}$  and  $R_s$ , respectively, calculated from the experimental I-V curve measurements. For non-uniform distributions in  $I_{sc}$  and  $R_s$ , the bar graph showing percentage changes in module electrical parameters namely, MPP,  $I_{mpp}$  and  $V_{mpp}$  with respect to non-degraded parameters is given in Figure 7.

For both types of non-uniform degradation modelled in the simulation, the comparative analysis of the trend of change in electrical parameters has been performed to comprehend the trends observed during DIV analysis. The trend of change in  $I_{mpp}$  for non-uniform distribution of both encapsulant and metallization degradation has been the same as evident from Figure 7, that is, a positive change implying loss in the current generation. It is because encapsulant degradation hinders the transmission of incident irradiation while the metallization degradation hinders the collection of light generated current. Thus, both types of degradation modes lead to loss in  $I_{mpp}$ . However, the percentage change in  $V_{mpp}$  has been opposite in trend. Herein, for non-uniform degradation in encapsulant, the change in  $V_{mpp}$  is negative, while for non-uniform metallization degradation, the change in  $V_{mpp}$  is positive. The difference in the trend of  $V_{mpp}$  can be understood based on the biasing of series connected cells. Due to decrease in  $I_{mpp}$  caused by non-uniform distribution of encapsulant degradation, the series connected cells operate at lower efficiency. This causes the operating voltage of cells, that is,  $V_{mpp}$  to move towards the  $V_{oc}$  leading to increase in cumulative module  $V_{mpp}$ . However, for non-uniform increase in  $R_s$ , prominently caused by metallization degradation, cells operate under reverse bias condition, resulting in decrease in the module  $V_{mpp}$ .

Under external operating conditions, various D&Ds modes operate simultaneously in the modules, thereby the percentage change in the electrical parameters would reflect the cumulative effect of existing D&Ds modes. In this section, with the help of simulations, the

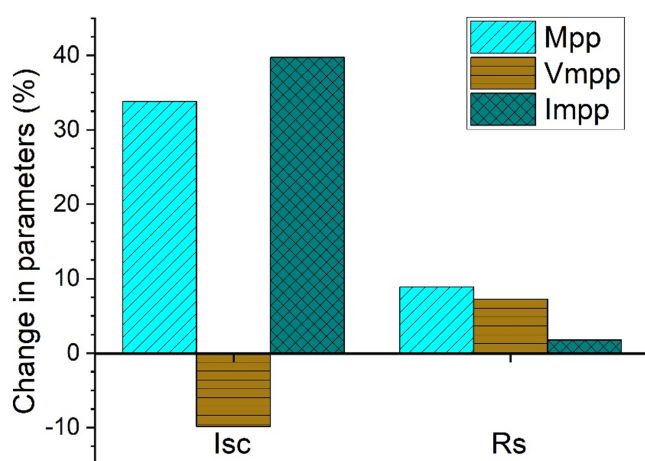


**FIGURE 7** Simulated percentage change in MPP,  $I_{mpp}$  and  $V_{mpp}$  for non-uniform  $I_{sc}$  and  $R_s$  in the cells of the PV module

independent effect of the most prominent degradations modes on the electrical parameters has been identified. As observed through simulations, encapsulant and metallization degradation both cause positive trend of percentage change in  $I_{mpp}$  and MPP of the module. However, the percentage change in  $V_{mpp}$  has positive trend in case of metallization degradation, while the trend is negative due to encapsulant degradation. Thus, in this work, the cumulative percentage change in  $V_{mpp}$  has been used to identify and qualitatively differentiate between the impact of encapsulant and metallization degradation in the solar cells of modules. In this regard, cells showing a positive trend in  $V_{mpp}$  change during DIV measurements imply that the influence of metallization degradation has been higher in the cells, whereas cells showing a negative trend in  $V_{mpp}$  change imply a higher extent of prominent encapsulant degradation, that is, discoloration over the cell.

### 3.3 | Correlation of DIV results with degradation modes

The analysis of simulation results show that the changes in  $V_{mpp}$  due to non-uniform degradation in the modules can be useful criteria in identifying the dominant degradation modes, wherein the percentage change in  $V_{mpp}$  depends on the type of D&Ds present in the cell. For non-uniform encapsulant degradation, the change in  $V_{mpp}$  has been negative, while for non-uniform distribution of metallization degradation in the cells, the percentage change in  $V_{mpp}$  has been positive. As such, the cumulative change in  $V_{mpp}$  in the presence of both encapsulant degradation and metallization degradation in a cell would depend on the dominant degradation mode. Thus, the trend of change in operating voltage, that is,  $V_{mpp}$ , during DIV analysis can be used to determine the major mode of degradation in a solar cell. During DIV analysis, the extent of non-uniformity in encapsulant degradation has been estimated from the percentage change in  $I_{sc}$  as discussed in Section 3.2.1. However, at operating conditions, that is, MPP, the trend of change in the electrical parameters would be due to the cumulative effect of both encapsulant and metallization degradation in the cell. Herein, based on the understanding developed from simulation results and the analysis of electrical parameters during DIV measurements, the trend of change in  $V_{mpp}$  has been corroborated with the prominent D&Ds identified in the cells of module.

For investigated modules, the cells showing maximum positive change in the  $V_{mpp}$  have been identified. In addition, the trend of change in MPP has also been analysed. It can be observed that the trend of change in MPP has been following the trend of change in  $V_{mpp}$ . It implies that the change in MPP has been dependent on the change in  $V_{mpp}$  during DIV analysis. For the module FA-01, cell-7 has shown the maximum positive  $V_{mpp}$  change and high positive MPP change as well. During cross-characterization for the same, finger corrosion at the cell edges, interruption in the fingers and discoloration have been observed through visual analysis and EL images as shown in Figure 8A. The presence of interruptions (encircled in blue) in multiple fingers affects the current collection and hence contributes to an

increase in  $R_s$  of the cell. Moreover, the dark region in EL images along the cell edges (encircled in red) corresponds with finger corrosion. Electrochemical reaction causing the corrosion of the fingers results in formation of non-conductive material, which restricts the collection of current through effected fingers. Also, the EL images of cell-7 show the presence of non-uniform discoloration. However, based on the cross-characterization results, it can be said that high  $R_s$  causing degradations due to finger corrosion and interruptions has higher impact in the cell-7 which can also be observed through the trend of positive  $V_{mpp}$  change.

Similarly, in the module FA-02, the trend of percentage change in MPP is positive for the majority of the solar cells; however, the change in  $V_{mpp}$  is negative. The change in  $V_{mpp}$  can be attributed to the cumulative effect of both non-uniform encapsulant degradation and metallization degradation. From the graph of  $V_{mpp}$  in Figure 8B, it can be observed that some of the peaks in the graph are moving towards the zero axis, indicating that the impact of  $R_s$  effecting anomalies is greater for the corresponding cells than the encapsulant degradation. This is also evident from the visual and microscopic inspection of the module. Figure 8B shows the visual and microscopic image of cell-19 of FA-02 module, which has shown maximum positive percentage change in  $V_{mpp}$  as well as in MPP, wherein brown-coloured deposition can be observed on the busbar ribbon. Moreover, the extent of discoloration was low in this cell as evident from visual image. Thus, for FA-02, also the presence of metallization degradation corresponding with high  $R_s$  agrees with the positive trend of change in  $V_{mpp}$  for cell-19.

Similar analysis of trend of change in  $V_{mpp}$  and MPP for the module FA-03 shows that the trend of change in these parameters for its two submodules has been distinct as can be observed in Figure 8C, wherein, for the submodule-I, the change in  $V_{mpp}$  is comparatively less negative or positive for some cells, correspondingly the change in MPP is positive for all the cells. While for submodule-II, the trend of change in  $V_{mpp}$  is negative for all its cells; correspondingly, the trend of change in MPP is negative for majority of cells. The visual and microscopic inspection of the FA-03 shows only the presence of non-uniform discoloration over the cells of the module. However, its EL image as shown in Figure 8C has a significant dark region over its solar cells. Moreover, the pattern as well as the area of the dark region is different in submodule-I compared to submodule-II. It can be attributed to non-uniform degradation amongst two submodules. Under external environment conditions, modules have been found to degrade at different rates even when installed and operating under the same external stresses.<sup>13</sup> Thus, different types of degradation modes can induce and accelerate at different pace within different cells of a module.

The detailed analysis of EL image of cell-14 (white enclosure) in submodule-I as shown in Figure 8C shows that the region around the busbar is dark while the region between the busbar is bright. However, visual inspection of cell-14 does not reveal presence of any degradation characteristic to the dark pattern in the EL image. Literature survey shows that such a pattern in EL imaging has been reported to occur due to the tin-migration related degradation of solder material

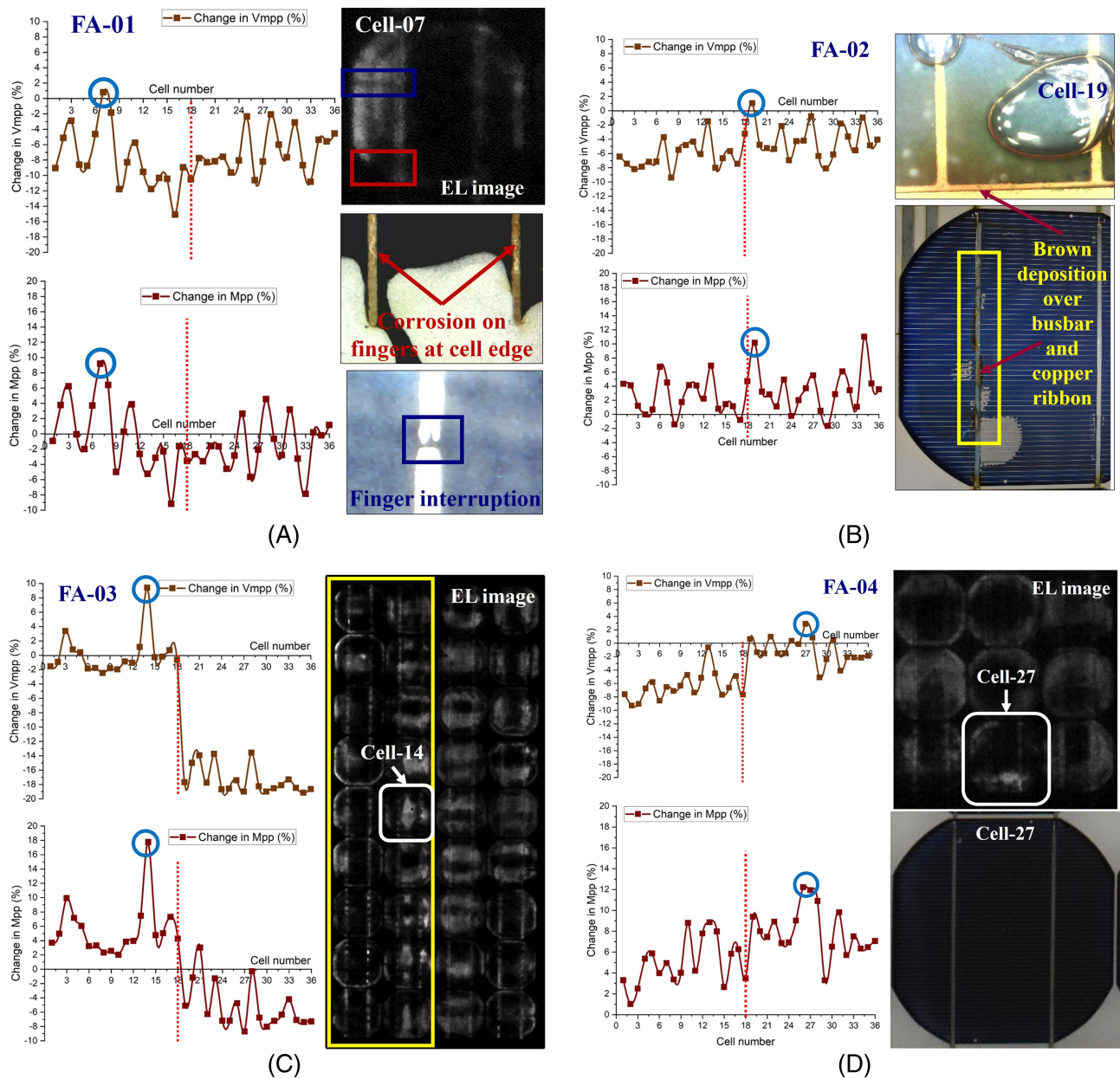


**FIGURE 8** Correlating results of DIV measurements with microscopic and EL images for module (A) FA-01, (B) FA-02, (C) FA-03 and (D) FA-04

from beneath busbar-ribbon assembly.<sup>44</sup> In the presence of air, moisture and high temperature conditions, tin material from solder material has been reported to undergo electro-chemical degradation, wherein the tin material in the form of whiskers migrates in the surrounding region having moisture. These tin whiskers have been found deposited at the finger-silicon interface. Being non-conductive in nature, tin whiskers block the collection of current from silicon to fingers, thus providing a high resistance to the current flow. Due to the same reason, the effected region appears dark in EL images. The tin whiskers could not be detected during visual inspection as they are micron level in size making them difficult to be visible through bare eyes. The migration of tin effects the current collection from the solar cell which leads to an increase in  $R_s$  causing comparatively less negative change in  $V_{mpp}$  for submodule-I. In contrast, the dark pattern in

submodule-II is mainly due to non-uniform discoloration, which is responsible for negative change in  $V_{mpp}$ .

The trend of change in  $V_{mpp}$  and MPP patterns for module FA-04 is similar to that observed for module FA-02. However, the visual inspection does not show the presence of degradation over its cell as shown in Figure 8D. The positive change in MPP implies that the presence of degradation modes is similar to that observed in the module FA-03. However, the severity of degradation is higher than FA-03, based on the extent of change in its MPP curve. Thus, based on the above discussion, it can be concluded that the comparative analysis of the trend of percentage change in  $V_{mpp}$  can be used for qualitative analysis of the major mode of degradation in the modules, wherein the non-uniformity in the degradation can be investigated based on the extent of change in  $I_{sc}$  and  $V_{mpp}$  through DIV analysis.

## 4 | CONCLUSION

In this work, field-aged PV modules have been systematically investigated for the dominant degradation modes in the solar cells amid the non-uniform distribution of defects and degradations (D&Ds). For this purpose, a novel, non-destructive characterization approach has been developed using DIV curve measurement, wherein solar cells of the modules have been sequentially subjected to partial shading while measuring the I-V curve of the module. The trend of percentage change in the electrical parameters of the module during DIV measurements has been utilized to investigate and differentiate dominant degradation mode in the cells solely on the basis of I-V characteristics of the module. The prominent D&Ds identified in the investigated modules are encapsulant degradation, namely, discoloration and delamination; metallization degradation, namely, finger and busbar corrosion, solder material degradation, finger interruptions, interconnect ribbon burnout and corrosion; and micro-cracks. The investigated modules had a non-uniform distribution of various types of D&Ds, which have been investigated by cross-characterization using EL imaging and microscopic inspection. However, both aforementioned techniques have their limitations in identifying and differentiating dominant degradation mode amongst non-uniform D&Ds present in the cells of modules singlehandedly. In this regard, the DIV approach presented in this work has been able to identify the dominant D&Ds in the cells of module using only I-V curve measurement.

The non-uniform distribution of encapsulant degradation, prominently discoloration over the cells of modules, has been identified through the trend of percentage change in the short circuit current ( $I_{sc}$ ), wherein cells with higher extent of discoloration have shown lower percentage change in  $I_{sc}$  and vice versa. It has also been observed that submodules within a module had significantly varying extents of discoloration over the cells. In addition, a correlation has been established between the percentage change in voltage at the maximum power point ( $V_{mpp}$ ) of the module with the prominent degradation mode present in the cell. Herein, the positive trend in the  $V_{mpp}$  change has been attributed to the increase in the series resistance of the cell due to metallization degradation and micro-cracks, while the negative trend in  $V_{mpp}$  change has been attributed to the loss in  $I_{sc}$  due to discoloration on the solar cell. In the end, the results obtained from DIV analysis have been compared and substantiated with the findings of cross-characterization. The trend of percentage change in  $V_{mpp}$  during DIV measurements can be used for the investigation and identification of dominant degradation modes in the cells of the field-installed modules. The proposed method caters to the need of identifying modules, which have undergone non-uniform degradation. It will be useful for applying suitable O&M decisions to maintain PV system's performance. For this purpose, use of I-V curve tracers installed with module arrays in the PV plants can be exploited. The presented approach can be used for the investigation of commercial crystalline PV technologies like PERC, mono-crystalline and multi-crystalline. However, the extension of the presented approach for thin-film technology cells could be challenging owing to the 'integrated series connection' of the solar cells.

## CONFLICT OF INTEREST

The authors declare that they have no known competing financial interest or personal relationships that could have appeared to influence the work reported in this paper.

## DATA AVAILABILITY STATEMENT

The data that support the findings of this study are available from the corresponding author upon reasonable request.

## ORCID

Roopmati Meena  <https://orcid.org/0000-0001-6061-2912>

Manish Kumar  <https://orcid.org/0000-0003-2689-464X>

## REFERENCES

1. Rawat R, Chandel SS. Simulation and optimization of solar photovoltaic-wind stand alone hybrid system in hilly terrain of India. *Int J Renew Energy Res.* 2013;3:595-604.
2. Rawat R, Kaushik SC, Lamba R. A review on modeling, design methodology and size optimization of photovoltaic based water pumping, standalone and grid connected system. *Renew Sustain Energy Rev.* 2016;57:1506-1519. doi:[10.1016/j.rser.2015.12.228](https://doi.org/10.1016/j.rser.2015.12.228)
3. Kumar S, Meena R, Gupta R. Finger and interconnect degradations in crystalline silicon photovoltaic modules: a review. *Sol Energy Mater sol Cells.* 2021;230:111296. doi:[10.1016/j.solmat.2021.111296](https://doi.org/10.1016/j.solmat.2021.111296)
4. Sharma V, Chandel SS. Performance and degradation analysis for long term reliability of solar photovoltaic systems: a review. *Renew Sustain Energy Rev.* 2013;27:753-767. doi:[10.1016/j.rser.2013.07.046](https://doi.org/10.1016/j.rser.2013.07.046)
5. Rajput P, Tiwari GN, Sastry OS, Bora B, Sharma V. Degradation of mono-crystalline photovoltaic modules after 22 years of outdoor exposure in the composite climate of India. *Sol Energy.* 2016;135:786-795. doi:[10.1016/j.solener.2016.06.047](https://doi.org/10.1016/j.solener.2016.06.047)
6. de Oliveira MCC, Diniz Cardoso ASA, Viana MM, Lins VDFC. The causes and effects of degradation of encapsulant ethylene vinyl acetate copolymer (EVA) in crystalline silicon photovoltaic modules: a review. *Renew Sustain Energy Rev.* 2018;81:2299-2317. doi:[10.1016/j.rser.2017.06.039](https://doi.org/10.1016/j.rser.2017.06.039)
7. Sharma V, Chandel SS. A novel study for determining early life degradation of multi-crystalline-silicon photovoltaic modules observed in western Himalayan Indian climatic conditions. *Sol Energy.* 2016;134:32-44. doi:[10.1016/j.solener.2016.04.023](https://doi.org/10.1016/j.solener.2016.04.023)
8. Ndiaye A, Charki A, Kobi A, et al. Degradations of silicon photovoltaic modules: a literature review. *Sol Energy.* 2013;96:140-151. doi:[10.1016/j.solener.2013.07.005](https://doi.org/10.1016/j.solener.2013.07.005).
9. Tracy J, Gambogi W, Felder T, et al. Survey of material degradation in globally fielded PV modules. *Conf Rec IEEE Photovolt Spec Conf.* 2019; 874-879. doi:[10.1109/PVSC40753.2019.8981140](https://doi.org/10.1109/PVSC40753.2019.8981140)
10. Quintana MAA, King DLL, McMahon TJ, Osterwald CRR. Commonly observed degradation in field-aged photovoltaic modules. *Conf Rec IEEE Photovolt Spec Conf.* 2003;1436-1439. doi:[10.1109/pvsc.2002.1190879](https://doi.org/10.1109/pvsc.2002.1190879)
11. Kuitche JM, Pan R, Tamizhmani G. Investigation of dominant failure mode(s) for field-aged crystalline silicon PV modules under desert climatic conditions. *IEEE J Photovoltaics.* 2014;4(3):814-826. doi:[10.1109/JPHOTOV.2014.2308720](https://doi.org/10.1109/JPHOTOV.2014.2308720)
12. Singh R, Sharma M, Rawat R, Banerjee C. An assessment of series resistance estimation techniques for different silicon based SPV modules. *Renew Sustain Energy Rev.* 2018;98:199-216. doi:[10.1016/j.rser.2018.09.020](https://doi.org/10.1016/j.rser.2018.09.020)
13. Gxasheka AR, van Dyk EE, Meyer EL. Evaluation of performance parameters of PV modules deployed outdoors. *Renew Energy.* 2005; 30(4):611-620. doi:[10.1016/j.renene.2004.06.005](https://doi.org/10.1016/j.renene.2004.06.005)

14. Park NC, Jeong JS, Kang BJ, Kim DH. The effect of encapsulant discoloration and delamination on the electrical characteristics of photovoltaic module. *Microelectron Reliab*. 2013;53(9-11):1818-1822. doi: [10.1016/j.microrel.2013.07.062](https://doi.org/10.1016/j.microrel.2013.07.062)
15. Sinha A, Sastry OS, Gupta R. Nondestructive characterization of encapsulant discoloration effects in crystalline-silicon PV modules. *Sol Energy Mater sol Cells*. 2016;155:234-242. doi: [10.1016/j.solmat.2016.06.019](https://doi.org/10.1016/j.solmat.2016.06.019)
16. Gopalakrishna H, Sinha A, Dolia K, Jordan D, Tamizhmani G. Nondestructive characterization and accelerated UV testing of browned field-aged PV modules. *IEEE J Photovoltaics*. 2019;9(6):1733-1740. doi: [10.1109/JPHOTOV.2019.2927920](https://doi.org/10.1109/JPHOTOV.2019.2927920)
17. Pozza A, Sample T. Crystalline silicon PV module degradation after 20years of field exposure studied by electrical tests, electroluminescence, and LBIC. *Prog Photovoltaics Res Appl*. 2016;24(3):368-378. doi: [10.1002/pip](https://doi.org/10.1002/pip)
18. Mirzaei M, Mohiabadi MZ. A comparative analysis of long-term field test of monocrystalline and polycrystalline PV power generation in semi-arid climate conditions. *Energy Sustain Dev*. 2017;38:93-101. doi: [10.1016/j.esd.2017.01.002](https://doi.org/10.1016/j.esd.2017.01.002)
19. Yedidi K, Tatapudi S, Mallineni J, Knisely B, Kutiche J, Tamizhmani G. Failure and degradation modes and rates of PV modules in a hot-dry climate: results after 16 years of field exposure. 2014 IEEE 40th Photovolt Spec Conf PVSC 2014:3245-3247. doi: [10.1109/PVSC.2014.6925626](https://doi.org/10.1109/PVSC.2014.6925626).
20. Polverini D, Field M, Dunlop E, Zaaiman W. Polycrystalline silicon PV modules performance and degradation over 20years. *Prog Photovoltaics Res Appl*. 2013;21:1004-1015. doi: [10.1002/pip](https://doi.org/10.1002/pip)
21. Chandel SS, Nagaraju Naik M, Sharma V, Chandel R. Degradation analysis of 28 year field exposed mono-c-Si photovoltaic modules of a direct coupled solar water pumping system in western Himalayan region of India. *Renew Energy*. 2015;78:193-202. doi: [10.1016/j.renene.2015.01.015](https://doi.org/10.1016/j.renene.2015.01.015)
22. Chattopadhyay S, Dubey R, Kuthanazhi V, et al. Visual degradation in field-aged crystalline silicon PV modules in India and correlation with electrical degradation. *IEEE J Photovoltaics*. 2014;4(6):1470-1476. doi: [10.1109/JPHOTOV.2014.2356717](https://doi.org/10.1109/JPHOTOV.2014.2356717).
23. Bouraiou A, Hamouda M, Chaker A, et al. Experimental investigation of observed defects in crystalline silicon PV modules under outdoor hot dry climatic conditions in Algeria. *Sol Energy*. 2018;159:475-487. doi: [10.1016/j.solener.2017.11.018](https://doi.org/10.1016/j.solener.2017.11.018).
24. Schlothauer J, Jungwirth S, Köhl M, Röder B. Degradation of the encapsulant polymer in outdoor weathered photovoltaic modules: spatially resolved inspection of EVA ageing by fluorescence and correlation to electroluminescence. *Sol Energy Mater sol Cells*. 2012;102:75-85. doi: [10.1016/j.solmat.2012.03.022](https://doi.org/10.1016/j.solmat.2012.03.022)
25. Buerhop C, Schlegel D, Niess M, Vodermayer C, Weißmann R, Brabec CJ. Reliability of IR-imaging of PV-plants under operating conditions. *Sol Energy Mater sol Cells*. 2012;107:154-164. doi: [10.1016/j.solmat.2012.07.011](https://doi.org/10.1016/j.solmat.2012.07.011)
26. Meena R, Kumar S, Gupta R. Comparative investigation and analysis of delaminated and discolored encapsulant degradation in crystalline silicon photovoltaic modules. *Sol Energy*. 2020;203:114-122. doi: [10.1016/j.solener.2020.04.041](https://doi.org/10.1016/j.solener.2020.04.041)
27. Pascual J, Martínez-Moreno F, García M, Marcos J, Marroyo L, Lorenzo E. Long-term degradation rate of crystalline silicon PV modules at commercial PV plants: an 82-MWp assessment over 10 years. *Prog Photovoltaics Res Appl*. 2021;29(12):1-9. doi: [10.1002/pip.3456](https://doi.org/10.1002/pip.3456)
28. Tsanakas JA, Ha L, Buerhop C. Faults and infrared thermographic diagnosis in operating c-Si photovoltaic modules: a review of research and future challenges. *Renew Sustain Energy Rev*. 2016;62:695-709. doi: [10.1016/j.rser.2016.04.079](https://doi.org/10.1016/j.rser.2016.04.079)
29. Li X, Yang Q, Chen Z, Luo X, Yan W. Visible defects detection based on UAV-based inspection in large-scale photovoltaic systems. *IET Renew Power Gener*. 2017;11(10):1234-1244. doi: [10.1049/iet-rpg.2017.0001](https://doi.org/10.1049/iet-rpg.2017.0001)
30. Henry C, Poudel S, Lee SW, Jeong H. Automatic detection system of deteriorated PV modules using drone with thermal camera. *Appl Sci*. 2020;10(11):1-16. doi: [10.3390/app10113802](https://doi.org/10.3390/app10113802)
31. Grimaccia F, Leva S, Dolara A, Aghaei M. Survey on PV modules common faults after an O&M flight extensive campaign over different plants in Italy. *IEEE J Photovoltaics*. 2017;7(3):810-816. doi: [10.1109/JPHOTOV.2017.2674977](https://doi.org/10.1109/JPHOTOV.2017.2674977)
32. Alves Dos Reis Benatto G, Mantel C, Spataru S, et al. Drone-based daylight electroluminescence imaging of PV modules. *IEEE J Photovoltaics*. 2020;10(3):872-877. doi: [10.1109/JPHOTOV.2020.2978068](https://doi.org/10.1109/JPHOTOV.2020.2978068).
33. Koch S, Weber T, Sobottka C, Fladung A, Clemens P, Berghold J, Outdoor electroluminescence imaging of crystalline photovoltaic modules: comparative study between manual ground-level inspections and drone-based aerial surveys. 32nd Eur Photovolt sol Energy Conf Exhib. 2016:1736-1740.
34. Sastry OS, Saurabh S, Shil SK, et al. Performance analysis of field exposed single crystalline silicon modules. *Sol Energy Mater sol Cells*. 2010;94(9):1463-1468. doi: [10.1016/j.solmat.2010.03.035](https://doi.org/10.1016/j.solmat.2010.03.035)
35. Chattopadhyay S, Dubey R, Bhaduri S, et al. Correlating infrared thermography with electrical degradation of PV modules inspected in all-india survey of photovoltaic module reliability 2016. *IEEE J Photovoltaics*. 2018;8(6):1800-1808. doi: [10.1109/JPHOTOV.2018.2859780](https://doi.org/10.1109/JPHOTOV.2018.2859780)
36. Monteiro LG, Macedo WN, Cavalcante RL, et al. Field I-V curve measurements methodology at string level to monitor failures and the degradation process: a case study of a 1.42 MWp PV power plant. *IEEE Access*. 2020;8:226845-226865. doi: [10.1109/ACCESS.2020.3044832](https://doi.org/10.1109/ACCESS.2020.3044832)
37. Alers GB, Zhou J, Deline C, Hacke P, Kurtz SR. Degradation of individual cells in a module measured with differential IV analysis. *Prog Photovoltaics Res Appl*. 2011;19(8):977-982. doi: [10.1002/pip.1013](https://doi.org/10.1002/pip.1013)
38. Sarkar MNI. Effect of various model parameters on solar photovoltaic cell simulation: a SPICE analysis. *Renewables Wind Water, Sol*. 2016;3(1):3-9. doi: [10.1186/s40807-016-0035-3](https://doi.org/10.1186/s40807-016-0035-3)
39. Kumar M, Kumar A. An efficient parameters extraction technique of photovoltaic models for performance assessment. *Sol Energy*. 2017;158:192-206. doi: [10.1016/j.solener.2017.09.046](https://doi.org/10.1016/j.solener.2017.09.046)
40. Adothu B, Chattopadhyay S, Bhatt P, Hui P, Costa FR, Mallick S. Early-stage identification of encapsulants photobleaching and discoloration in crystalline silicon photovoltaic module laminates. *Prog Photovoltaics Res Appl*. 2020;28(8):767-778. doi: [10.1002/pip.3269](https://doi.org/10.1002/pip.3269)
41. Patel AP, Sinha A, Tamizhmani G. Field-aged glass/backsheet and glass/glass pv modules: encapsulant degradation comparison. *IEEE J Photovoltaics*. 2020;10(2):607-615. doi: [10.1109/JPHOTOV.2019.2958516](https://doi.org/10.1109/JPHOTOV.2019.2958516)
42. Mohammed Niyaz H, Meena R, Gupta R. Impact of cracks on crystalline silicon photovoltaic modules temperature distribution. *Sol Energy*. 2021;225:148-161. doi: [10.1016/j.solener.2021.07.038](https://doi.org/10.1016/j.solener.2021.07.038)
43. Meena R, Kumar S, Gupta R. Investigation and analysis of chemical degradation in metallization and interconnects using electroluminescence imaging in crystalline silicon photovoltaic modules. 2020 Conf Rec IEEE Photovolt Spec Conf. 2020;2020-June:2596-9. doi: [10.1109/PVSC45281.2020.9300539](https://doi.org/10.1109/PVSC45281.2020.9300539).
44. Kumar S, Meena R, Gupta R. Imaging and micro-structural characterization of moisture induced degradation in crystalline silicon photovoltaic modules. *Sol Energy*. 2019;194:903-912. doi: [10.1016/j.solener.2019.11.037](https://doi.org/10.1016/j.solener.2019.11.037)

**How to cite this article:** Meena R, Kumar M, Gupta R. Investigation of dominant degradation mode in field-aged photovoltaic modules using novel differential current-voltage analysis approach. *Prog Photovolt Res Appl*. 2022;30(11):1312-1324. doi: [10.1002/pip.3580](https://doi.org/10.1002/pip.3580)